High-efficiency, ultra low-noise all-fiber photon-pair source

Shellee D. Dyer, Martin J. Stevens, Burm Baek, and Sae Woo Nam

National Institute of Standards and Technology, Optoelectronics Division, 325 Broadway, Boulder, CO 80305 USA
ph.: 303-497-7463; FAX: 303-497-3387
sdyer@boulder.nist.gov

Abstract: We demonstrate an all-fiber photon-pair source with the highest coincidence-to-accidental ratio (CAR) reported to date in the fiber-optic telecom C-band. We achieve this through careful optimization of pair-production efficiency as well as careful characterization and minimization of all sources of background photons, including Raman generation in the nonlinear fiber, Raman generation in the single-mode fiber, and leakage of pump photons. We cool the nonlinear fiber to 4 K to eliminate most of the Raman scattering, and we reduce other noise photon counts through careful system design. This yields a CAR of 1300 at a pair generation rate of 2 kHz. This CAR is a factor of 12 higher than previously reported results in the C-band. Measured data agree well with theoretical predictions.

OCIS codes: (060.4370) Nonlinear optics, fibers; (190.4410) Nonlinear optics, parametric processes; (270.0270) Quantum optics.

References and links

1. Y. Shih, "Entangled biphoton source – property and preparation," Rep. Prog. Phys. **66**, 1009-1044 (2003).
2. X. Li, J. Chen, P. Voss, J. Sharping, and P. Kumar, "All-fiber photon pair source for quantum communications: improved generation of correlated photons," Opt. Express **12**, 3737-3744 (2004).
3. K. F. Lee, J. Chen, C. Liang, X. Li, P. L. Voss, and P. Kumar, "Generation of high-purity telecom-band entangled photon pairs in dispersion-shifted fiber," Opt. Lett. **31**, 1905-1907 (2006).
4. J. Chen, K. F. Lee, C. Liang, and P. Kumar, "Fiber-based telecom-band degenerate-frequency source of entangled photon pairs," Opt. Lett. **31**, 2798-2800 (2006).
5. C. Liang, K. F. Lee, M. Medic, P. Kumar, R. H. Hadfield, and S. W. Nam, "Characterization of fiber-generated entangled photon pairs with superconducting single-photon detectors," Opt. Express **15**, 1322-1327 (2007).
6. H. Takesue and K. Inoue, "1.5-μm band quantum-correlated photon pair generation in dispersion-shifted fiber: suppression of noise photons by cooling fiber," Opt. Express **13**, 7832-7839 (2005).
7. R. M. Shelby, M. D. Levenson, S. H. Perlmutter, R. G. DeVoe, and D. F. Walls, "Broad-band parametric deamplification of quantum noise in an optical fiber," Phys. Rev. Lett. **57**, 691-694 (1986).
8. J. Fan, A. Dogariu, and L. J. Wang, "Generation of correlated photon pairs in a microstructure fiber," Opt. Lett. **30**, 1530-1532 (2005).
9. J. Fan, A. Migdall, and L. J. Wang, "Efficient generation of correlated photon pairs in a microstructure fiber," Opt. Lett. **30**, 3368-3370 (2005).
10. J. Fan and A. Migdall, "A broadband high spectral brightness fiber-based two-photon source," Opt. Express **15**, 2915-2920 (2007).
11. J. G. Rarity, J. Fulconis, J. Duligall, W. J. Wadsworth, and P. St. J. Russell, "Photonic crystal fiber source of correlated photon pairs," Opt. Express **13**, 534-544 (2005).
12. K. Garay-Palmett, H. J. McGuinness, O. Cohen, J. S. Lundeen, R. Rangel-Rojo, A. B. U'Ren, M. G. Raymer, C. J. McKinstrie, S. Radic, and I. A. Walmsley, "Photon pair-state preparation with tailored spectral properties by spontaneous four-wave mixing in photonic-crystal fiber," Opt. Express **15**, 14870-14886 (2007).
13. Q. Lin, F. Yaman, and G. P. Agrawal, "Photon-pair generation in optical fibers through four-wave mixing: role of Raman scattering and pump polarization," Phys. Rev. A **75**, 023803 (2007).
14. G. P. Agrawal, *Nonlinear Fiber Optics* (Academic Press, 2007), Chap. 10.
15. S. E. Mechels, J. B. Schlager, and D. L. Franzen, "Accurate measurements of the zero-dispersion wavelength in optical fibers," J. Res. Natl. Inst. Stand. Technol. **102**, 333-347 (1997).

#95442 - $15.00 USD Received 28 Apr 2008; revised 6 Jun 2008; accepted 16 Jun 2008; published 20 Jun 2008

1. Introduction

Photon-pair sources have exciting applications as entangled photon-pair generators or as heralded sources of single photons in fields such as linear optical quantum computing, entanglement-based quantum key distribution, and metrology. Historically, photon pairs were generated from spontaneous parametric down conversion (SPDC) in free-space nonlinear crystals and atoms [1], but more recently pair generation from four-wave mixing (FWM) in optical fiber has generated strong interest [2-6]. Photon-pair generation in optical fiber has many advantages, including compatibility with existing fiber telecommunications networks and low-loss coupling to single-photon counting detectors. Another key advantage of our all-fiber photon pair source is its compact and portable design.

For optimal long-distance transport of fiber pairs, it is necessary to create photons within the low-loss window (telecom C-band, with wavelengths near 1550 nm) of optical-fiber networks. Additionally, operating in the C-band opens up the possibility of using off-the-shelf optical filters that were designed for telecommunications applications, as an inexpensive and readily available alternative to custom-designed filters. The efficiency of FWM in optical fiber is directly related to the dispersion of the fiber, with the highest efficiency occurring near the zero-dispersion wavelength (ZDW) of the fiber. Most conventional single-mode fibers have ZDW near 1300 nm; achieving a ZDW near 1550 nm requires a specialty fiber such as dispersion-shifted fiber (DSF), highly nonlinear fiber (HNLF) or microstructured fiber.

One problem with fiber-based photon-pair sources is the strong spontaneous Raman scattering that occurs in the fiber. It has previously been demonstrated that the Raman scattering can be suppressed by cooling the nonlinear fiber in liquid nitrogen to 77 K [3,6]. Additionally, [7] demonstrated that by cooling the nonlinear fiber to 4 K it was possible to achieve squeezed states with noise levels below the standard quantum limit. Here we achieve almost complete suppression of Raman photons by cooling the fiber in liquid helium to 4 K. However, elimination of the Raman scattering in the nonlinear fiber is not sufficient to achieve optimal performance. We therefore carefully characterize and reduce all other background photon counts, including those from Raman scattering in the short lengths of uncooled conventional fiber and photon leakage from the pump lasers. These background signals are small compared with the Raman contribution when the nonlinear fiber is at temperatures of 77 K or higher, but when the Raman scattering is almost entirely extinguished at 4 K, these additional background contributions are the dominant noise signals.

An alternative for achieving high CAR with cryogenic cooling of the fiber is to use microstructure or photonic crystal fiber [8-12]. These fibers have single-mode transmission over a broad wavelength range, and therefore the Raman generation can be reduced through a wide detuning between the pump and the signal and idler wavelengths. Using microstructure fiber, a photon pair source with a CAR higher than 1000 has been demonstrated [10], but the generated photon pairs were outside of the desirable telecommunication C-band wavelength range.

A detailed theory that describes spontaneous FWM and Raman scattering in optical fiber was recently published in [13]. That paper, combined with formulas and derivations from [14], predicts the photon-pair and Raman photon generation rates based on the fiber nonlinearity, ZDW, dispersion slope, Raman gain, and filter bandwidths and center wavelengths. Combining the predictions of photon-pair generation rate from [13] with the detection efficiency (DE) of the detectors yields the predicted photon-pair detection rate. In this paper, we describe how we characterize the fiber parameters. We also show agreement between measured data and the predictions based on [13].

#95442 - $15.00 USD Received 28 Apr 2008; revised 6 Jun 2008; accepted 16 Jun 2008; published 20 Jun 2008

2. Nonlinear fiber characterization using stimulated four wave mixing

In this section we describe how we characterized the nonlinear fiber using stimulated FWM in order to find the optimal pump wavelength, which is determined by the properties of the nonlinear fiber, specifically its nonlinear coefficient, zero-dispersion wavelength, and the dispersion slope. The stimulated FWM measurement system is shown in Fig. 1. In this experiment we have two CW tunable lasers: a "pump" laser and a "probe" laser. We include a polarization controller so that we can match the polarization states of the two lasers, an essential step for optimal FWM. A fiber optic beamsplitter combines the light from the two lasers; that light then propagates through 0.3 km of DSF, and we measure the output spectrum on an optical spectrum analyzer (OSA). The pump laser is amplified with an erbium-doped fiber amplifier to achieve a power of 24.5 mW, while the probe laser power is set to 1.0 mW; both are measured with a power meter as shown in Fig. 1.

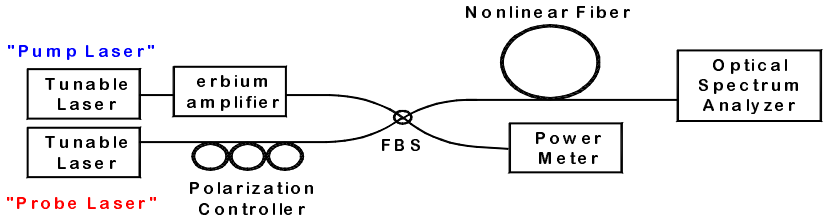

Fig. 1. Diagram of the stimulated four-wave mixing experiment used to characterize the nonlinear fiber and determine the optimal pump wavelength. FBS = fiber optic beamsplitter.

From energy conservation, we have

$$2\omega_p = \omega_s + \omega_i \,, \tag{1}$$

where ω_p and ω_s are the frequencies of the pump and probe lasers, respectively, and ω_i is the frequency of the generated idler photons. We measure the ratio of the intensity of the four-wave mixing component to the intensity of the probe on the OSA. Under the undepleted pump approximation, that ratio, which is called the FWM efficiency, is estimated by [14]

$$\frac{P_i(L)}{P_s(L)} \approx \frac{P_i(L)}{P_s(0)} = \left(1 + \frac{\kappa^2}{4|g|^2}\right)\left|\sinh(gL)\right|^2 , \tag{2}$$

where L is the length of the nonlinear fiber, P_i is the power of the generated photons at the idler wavelength, g is the parametric gain, and P_s is the power at the probe laser wavelength, which we assume is large compared with P_i for all L, i.e., the power from the probe laser is much stronger than the power generated through FWM. We are also assuming perfect alignment of the polarization states of the pump and probe lasers. The effective phase mismatch κ is given by

$$\kappa = k_s + k_i - 2k_p + 2\gamma P_0 = \Delta k + 2\gamma P_0 \,, \tag{3}$$

where k_s, k_i, and k_p are the signal, idler and pump wave vectors, respectively, P_0 is the pump power, and γ is the nonlinear coefficient of the fiber. The Δk term of Eq. (3) can be approximately related to the dispersion of the nonlinear fiber as

$$\Delta k \approx \beta_2 \Omega_s^2 \,, \tag{4}$$

#95442 - $15.00 USD Received 28 Apr 2008; revised 6 Jun 2008; accepted 16 Jun 2008; published 20 Jun 2008

where β_2 is the group-velocity parameter (equal to $d^2\beta/d\omega^2$, where β is the fiber propagation constant) and Ω_s is the radial frequency difference between the pump and the signal or idler. We approximate the group velocity parameter β_2 as a linear function: $\beta_2 \approx m\Delta\lambda_{ZD}$, where m is the slope and $\Delta\lambda_{ZD}$ is the difference between the pump wavelength and the zero-dispersion wavelength ($\Delta\lambda_{ZD} = \lambda_p - ZDW$). Note that this linear approximation will not work well with specialty fiber such as dispersion flattened fiber; in that case we would approximate β_2 as a quadratic or even cubic function of $\Delta\lambda_{ZD}$, but for DSF and assuming a small $\Delta\lambda_{ZD}$, a linear approximation is sufficient.

The parametric gain is given by

$$g^2 = (\gamma P_0)^2 - (\kappa/2)^2 . \tag{5}$$

Using Eq. (5), we can rewrite Eq. (2) as

$$\frac{P_i(L)}{P_s(L)} \approx (\gamma P_0 L)^2 \left| \frac{\sinh(gL)}{gL} \right|^2 . \tag{6}$$

We measure the FWM efficiency by dividing the power at the idler frequency by the power at the signal frequency; both powers are measured on the OSA. We repeat this measurement as we tune both the pump and probe lasers, keeping the detuning between the two lasers fixed at 5 nm. The results are shown in Fig. 2 for three fiber temperatures: room temperature, cooled to 77 K by immersing the fiber in a liquid nitrogen bath, and cooled to 4 K by immersing the fiber in liquid helium.

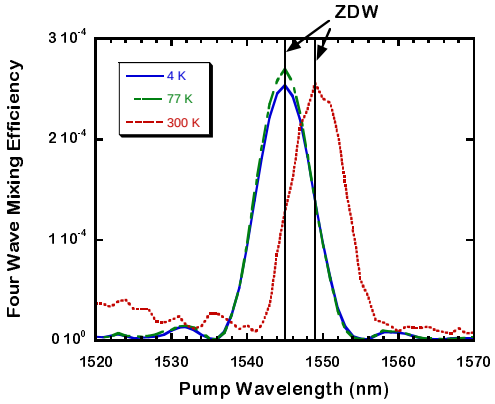

Fig. 2. Plot of the measured stimulated FWM efficiency as a function of the pump wavelength for three different temperatures of the nonlinear fiber: 300 K, 77 K, and 4 K.

We determine γ, m, and ZDW by fitting the data of Fig. 2 to Eqs. (3) - (6). We obtain γ = 2.2 $W^{-1} \cdot km^{-1}$, m = -0.12 $ps^2 \cdot nm^{-1} \cdot km^{-1}$, ZDW (T = 4 K) = ZDW (T = 77 K) = 1544.8 nm, and ZDW (T = 300 K) = 1549 nm. Previously, the temperature coefficient of the ZDW of DSF was reported to be 0.03 nm/K, but that was based on measurements near room temperature [15]. To our knowledge, no one has reported the change in ZDW at cryogenic temperatures. We find that the ZDW changes by only 4 nm when the fiber is cooled to 77 K, and we see no significant change in ZDW between 77 K and 4 K. We also find that the change in dispersion slope m with temperature was negligible, as predicted by [15].

#95442 - $15.00 USD Received 28 Apr 2008; revised 6 Jun 2008; accepted 16 Jun 2008; published 20 Jun 2008

In Fig. 2 we see that the maximum FWM efficiency occurs when the pump wavelength is very close to the ZDW. Ideally, we should pump at the wavelength that yields maximum FWM efficiency; but practically, if we limit our pump wavelength to the ITU (International Telecommunication Union) standard grid wavelengths, which are separated by approximately 1.6 nm, it is unlikely that we will be able to achieve maximum FWM efficiency. However, from Fig. 2, we see that a ~ ± 1.6 nm detuning from the optimal wavelength yields little change in FWM efficiency.

3. Spontaneous FWM and photon pair generation

In the previous section we determined the properties of the nonlinear fiber using stimulated FWM. In this section we describe how we use the parameters obtained from that characterization to design a high-efficiency photon pair source. Here we are no longer using a probe laser, and we replace the CW pump laser of the stimulated FWM measurement with a high-power pulsed laser to generate photon pairs through spontaneous FWM in the nonlinear fiber, a process in which two pump photons interact with vacuum fluctuations in the fiber to create a signal and idler photon pair.

We choose the frequencies of the pump, signal and idler filters from the standard ITU grid, which allows us to use inexpensive, mass-produced components. Here we use a pump wavelength of 1546.1 nm. As shown in Fig. 2, this is very close to the pump wavelength that gives the maximum FWM efficiency for cryogenically cooled fiber, but yields a less-than-optimal FWM efficiency at room temperature.

A diagram of the photon pair source is shown in Fig. 3. The pump laser is a femtosecond fiber laser with a repetition rate of 36 MHz. We filter it with a 1 nm linewidth tunable filter, designed to pass the pump wavelength. We then amplify the filtered pump with an erbium-doped fiber amplifier (EDFA). The EDFA contributes unwanted photons in the form of amplified spontaneous emission (ASE), and therefore we include a post-amplification bandpass filter at the pump wavelength. A variable attenuator enables investigations of the effects of pump power. We also include another stage of bandpass filtering at the pump wavelength prior to and as close as possible to the DSF for reasons that will be explained below. The photon pairs are generated through spontaneous FWM in the DSF, and then the signal and idler photons are separated from pump photons by a series of signal and idler filters. The outputs of these filters are coupled to a pair of superconducting single-photon detectors with system quantum efficiencies (QEs) of 0.32 % and 1.6 % and dark count rates of 100 Hz.

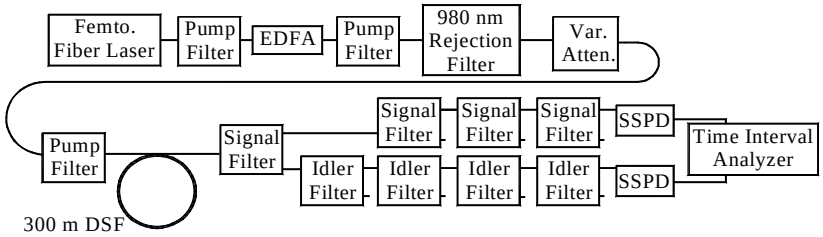

Fig. 3. Diagram of the photon pair generation source. DSF = dispersion shifted fiber. EDFA = erbium-doped fiber amplifier. SSPD = superconducting single-photon detectors. The pump filters are all bandpass filters with 1 nm linewidth at a center wavelength of 1546.1 nm. The signal and idler filters are also bandpass filters with 1 nm linewidth at the signal and idler wavelengths.

The expected detected intensity resulting from photon pair generation is given approximately by [13]

#95442 - $15.00 USD Received 28 Apr 2008; revised 6 Jun 2008; accepted 16 Jun 2008; published 20 Jun 2008

$$I_{pair,u} \approx \eta_u \Delta\nu D_c \left(\gamma P_0 L\right)^2 \left|\frac{\sinh\left(gL\right)}{gL}\right|^2, \tag{7}$$

where η_u is the effective detection efficiency, which includes both detector quantum efficiency and the insertion loss of the signal or idler filters, $\Delta\nu$ is the bandwidth of the signal and idler filters (which we model as perfect rect functions with equal bandwidths), P_0 is the peak power, and D_c is the duty cycle of the pump laser. The subscript u is replaced with i for idler photons and s for signal photons. Here we use the undepleted pump approximation, and we neglect the Raman contribution to the nonlinear phase shift (i.e., $f_R \approx 0$) [13]. Also, we are neglecting cross-polarized pair generation, so that all photon pairs are modeled as being co-polarized with the pump [13]. The parametric gain g is given by Eq. (5). For low pump powers and small $\Delta\lambda_{ZD}$, the gL term of Eq. (7) is small, and therefore we can make the approximation that $\sinh(gL)/gL \approx 1$. In that case, Eq. (7) above is consistent with Eq. (22) of [13].

It is also helpful to compare Eq. (7) with Eq. (6). With the exception of a proportionality constant, these equations are identical, which means that the stimulated FWM experiment can be used to predict directly the photon-pair generation rate as a function of pump wavelength. In this comparison we neglected any change in pump power between the stimulated and spontaneous FWM experiments other than the change in duty cycle, and this approximation is always true near the ZDW, where $g \approx 0$. This assumption is also valid for low pump powers and large detunings, where $g \approx i\Delta k/2$. In both of these cases (either $g \approx 0$ or $g \approx i\Delta k/2$), we can approximate the pair generation rate of Eq. (7) as quadratic with pump power.

4. Characterizing the Raman contribution

In the previous two sections, we described how we optimized photon-pair generation. In this section, we describe the effects of spontaneous Raman scattering in the fiber, which can be a significant problem for fiber-based photon-pair generation. We describe formulas used to predict the Raman contribution as well as measurements to characterize it.

The expected detected intensity resulting from Raman generation is given approximately by [13]

$$I_R \approx \eta_u \Delta\nu P_0 L D_c \left|g_R\right| \mathrm{N}\left(\Omega_s\right) = \eta_u \mu_b\left(\Omega_s\right) f_p, \tag{8}$$

where g_R is the Raman gain, which is determined by the properties of the fiber as well as from the detuning $\Omega_s = \omega_s - \omega_p = \omega_p - \omega_i$, μ_b is defined as the probability of a Raman count per pulse, and f_p is the repetition frequency of the pump laser. The phonon population is predicted by

$$\mathrm{N}\left(\Omega_s\right) = \begin{cases} \varphi(T,\Omega_s) & \text{for } \omega > \omega_p, \\ \varphi(T,\Omega_s)+1 & \text{for } \omega < \omega_p, \end{cases} \tag{9}$$

where

$$\varphi(T,\Omega_s) = \left[\exp\left(\frac{\hbar\left|\Omega_s\right|}{k_B T}\right) - 1\right]^{-1} \tag{10}$$

is the Bose-Einstein temperature-dependant correction factor. From Eq. (10) it is clear that the phonon population depends strongly on temperature T. The difference of + 1 between the Stokes and anti-Stokes components of the Raman scattering in Eq. (9) reflects the fact that energy can still be transferred to the fiber when it is cooled near absolute zero. This + 1 difference between Stokes and anti-Stokes scattering is negligible at room temperature where $\varphi(T,\Omega_s) \approx 9$ (assuming $\Omega_s \approx 4$ THz, corresponding to a 5 nm detuning), but at T = 4 K where

#95442 - $15.00 USD Received 28 Apr 2008; revised 6 Jun 2008; accepted 16 Jun 2008; published 20 Jun 2008

$\varphi(T,\Omega_s) \approx 0.0005$, it creates a substantial difference between the Stokes and anti-Stokes scattering.

The Raman intensity generally increases with Ω_s until it peaks near 15 THz, which corresponds to a wavelength detuning of 120 nm at a center wavelength of 1550 nm [13]. This frequency detuning is too large for low-loss transmission in conventional fiber. Therefore, we reduce the Raman contribution by minimizing the frequency detuning as much as practically possible, but at room temperature there remains a large Raman contribution.

We are able to almost entirely eliminate the Raman scattering in the DSF by cooling it to 4 K in liquid helium. However, there is a small Raman contribution from the short length of uncooled single-mode fiber (SMF) that connects the last pump bandpass filter to DSF and the DSF to the first of the signal and idler bandpass filters. This length of fiber is very short (less than 20 m) compared with the length of the DSF, and the Raman scattering in this short length of SMF is not noticeable compared to the Raman scattering in the DSF at temperatures higher than 4 K. However, at 4 K the Raman scattering in uncooled SMF becomes the dominant background term. We minimize this by reducing the length of SMF pigtails on the last pump filter and the first of the signal and idler filters, but we cannot entirely eliminate these pigtails. We measured the effects of Raman scattering in SMF by replacing the DSF with extra lengths of SMF in increments of 30 m, up to a total length of 120 m. The measured count rates as a function of pump power are shown in Fig. 4(a), along with the linear curve fits to each data set. Figure 4(b) shows the slopes of each of the curves of Fig. 4 (a) as a function of the length of added SMF. Also shown in Fig. 4(b) is a curve fit to that data; from the slope and intercept of this fit and from Eqs. (8) - (10), we determine both the Raman gain ($g_R = 0.03\ W^{-1} \cdot km^{-1}$) and the combined length (15 m) of the SMF pigtail of the last pump filter and the SMF pigtail of the first of the signal and idler filters. However, we believe that the actual length of these SMF pigtails is somewhat shorter than this measurement indicates (no longer than 8 m). It is possible that some small percentage of pump photons are leaking through the signal and idler filters and being misidentified as Raman photons generated in the SMF in this measurement.

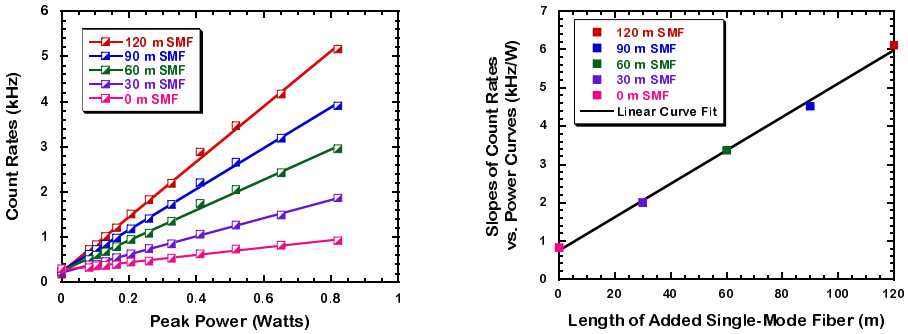

Fig. 4. Detector count rates resulting from Raman scattering in the SMF that connects the last pump filter and the first of the signal and idler filters. (a) We measured the count rates versus peak pump power for increasing lengths of additional SMF. Also shown are the linear curve fits for each SMF length. To avoid confusion, measurements are shown for only one of the two detector channels in the system. (b) Slopes of the curves from (a) with a linear curve fit. From the linear curve fit, we can determine the Raman coefficient and length of the SMF pigtails of the last pump filter and the first of the signal and idler filters.

We also characterized the Raman gain of the DSF by measuring count rates as a function of pump power with the fiber at room temperature, shown in Fig. 5 for the two different

#95442 - $15.00 USD Received 28 Apr 2008; revised 6 Jun 2008; accepted 16 Jun 2008; published 20 Jun 2008

superconducting single photon detectors (SSPD) channels. With the DSF in place, the count rate function is no longer linear, but now includes quadratic and possibly higher-order terms as described by Eq. (7). We fitted a quadratic curve to the data, as shown in Fig. 5. We calculate the Raman gain of the DSF from the linear term of the quadratic fit, after subtracting the contribution of the SMF that connects the last pump filter to the first of the signal and idler filters. We obtain a Raman gain of $g_R = 0.08\ \mathrm{W^{-1} \cdot km^{-1}}$ for the DSF.

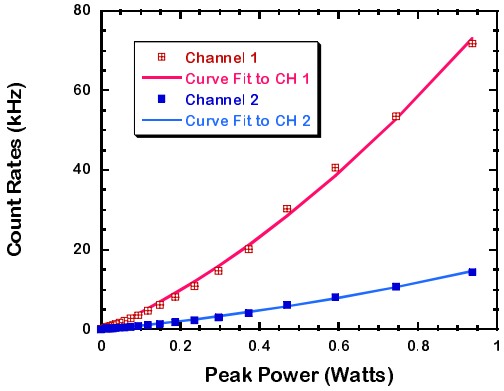

Fig. 5. Count rate versus pump power curve with quadratic curve fits. We use these curve fits to characterize the Raman gain of the DSF. The large difference between these two curves reflects the large difference in the quantum efficiency of the two detectors.

5. Minimizing other sources of background photons

In the previous section we described how to characterize and minimize the Raman scattering. In this section we discuss other sources of background photons. These background counts are generally weak compared to Raman scattering, except in the case where the nonlinear fiber is cooled to 4 K and the Raman contribution is almost eliminated.

One concern is leakage of pump photons; we characterized this by removing the DSF and measuring the photon counts at the two detectors. In choosing the signal and idler wavelengths, we restrict ourselves to the ITU grid wavelengths, which are separated by about 1.6 nm. We found unacceptable pump leakage for detunings less than 3 ITU channels (4.8 nm) from the pump wavelength. Therefore, we chose signal and idler wavelengths of 1550.92 and 1541.35 nm, a spacing of 3 ITU channels from the pump. Using Eq. (7), we can estimate the pump-wavelength rejection required to reduce the leakage of pump photons to 1 % of the expected photon-pair generation rate. Assuming that the pump filters have perfect rect profiles as functions of wavelength, we calculate that we need 101 dB of pump rejection, which can be achieved by cascading multiple bandpass filters at the signal and idler wavelengths. However, it is also desirable to minimize the number of filters in the cascade, as each filter will add insertion loss to the system, lowering the effective DE of the detectors and increasing the integration time required to obtain good statistics. These filters specify around 1 dB insertion loss per filter, with at least 30 dB adjacent channel isolation and even higher isolation expected at non-adjacent channels. We compared the detector count rates measured with a cascade of 3, 4 and 5 filters at the signal and idler wavelengths. We found that the cascade of 4-filters offered measurable improvement in the pump rejection compared to a 3-filter cascade, but that the 5-filter configuration did not reduce the count rate compared to a 4-filter cascade by more than the insertion loss of the additional filter. Therefore, we use a cascade of 4 filters each at the signal and idler wavelengths, giving a total insertion loss of 4.5 dB per channel. This 4-filter cascade provides more than 120 dB rejection of the pump,

#95442 - $15.00 USD Received 28 Apr 2008; revised 6 Jun 2008; accepted 16 Jun 2008; published 20 Jun 2008

which is noticeably larger than our estimate of required pump rejection above; this difference likely arises from our model of the pump filters as perfect rect functions.

Another source of leakage photons is the 980 nm photons originating from the high-power laser diodes that pump both the femtosecond fiber laser and the EDFA. The pump filters are designed for photons near 1550 nm; therefore, they are not necessarily effective at eliminating 980 nm photons. The leakage of 980 nm photons is not noticeable unless the Raman contribution is almost eliminated by cooling the DSF to 4 K. We filter these 980 nm photons by adding a dichroic fiber beamsplitter to the pump filter chain.

6. Comparison of predicted and measured coincidence-to-accidental ratios

In Secs. 4 and 5 we described the types of noise photons and how we characterized and minimized them. In this section we discuss how we characterize the photon pair-generation system of Fig. 3 as a whole, comparing the rate of desired photon-pair generation to the noise photon rate in terms of the coincidence-to-accidental ratio (CAR).

We estimate the expected CAR by first calculating the probability of detecting a coincidence count from pair generation in a given laser pulse from Eq. (7) as

$$C \approx \eta_1 \eta_2 \frac{\Delta\nu \; D_c \left(\gamma P_0 L\right)^2}{f_p} \left| \frac{\sinh\left(gL\right)}{gL} \right|^2 = \eta_1 \eta_2 \mu \,, \tag{11}$$

where μ is defined as the probability of a pair generation per pulse. The probability of detecting an accidental coincidence per pulse is approximated by

$$A \approx \eta_1 \eta_2 \left[\mu + \mu_{b,SMF,s} + \mu_{b,DSF,s} + \frac{p_d}{\eta_1} \right] \left[\mu + \mu_{b,SMF,i} + \mu_{b,DSF,i} + \frac{p_d}{\eta_2} \right], \tag{12}$$

where p_d is the probability that a dark count will occur in any sampling bin of the histogram, and the subscripts *s* and *i* distinguish between the Raman scattering at the signal and idler frequencies. The CAR is then calculated as *C/A*.

We measure the CAR as follows: the time-interval analyzer (TIA) shown in Fig. 3 records a histogram of the relative time delays between clicks recorded on detector 1 and clicks recorded on detector 2. Two example histograms are shown in Fig. 6: one histogram measured at room temperature (a), and one measured at 4 K (b). In Fig. 6(a), we see a series of peaks recurring at the repetition rate of the laser. The tallest peak includes the "true" coincidences, where each detector sees one-half of the same photon pair, as well as accidental coincidences, which occur for all the combinations and permutations of one-half of a photon pair, Raman photon, dark count, or one photon from a multiple photon pair registered at either detector, as summarized in Table 1. We estimate the accidentals from the average number of counts recorded in the non-zero-delay peaks. When we cool the fiber to 4 K, the Raman contribution is almost entirely eliminated, and the counts at all non-zero-delay peaks are reduced significantly, as shown in Fig. 6(b).

We estimate the CAR from the measured histogram using the total number of correlation counts in the zero-delay peak of the histogram divided by the average number of correlation counts in the non-zero-delay peaks. The TIA is not synchronized with the laser pulses; instead it samples the detector outputs at intervals of 128 ps. This distributes the correlation counts due to each laser pulse over three adjacent bins. We therefore integrate the correlation counts over three sampling bins to obtain the total number of correlation counts per laser pulse. Another effect of the 128 ps sampling interval is that it likely reduces the CAR slightly, because it is much broader than the 3 ps correlation time of our photon pairs, determined by the linewidths of the signal and idler filters. The 128 ps sampling interval degrades the measured CAR slightly by creating a longer window in which noise photons and dark counts can be detected and recorded as accidental counts. We included the effects of

#95442 - $15.00 USD Received 28 Apr 2008; revised 6 Jun 2008; accepted 16 Jun 2008; published 20 Jun 2008

the sampling interval in our simulations by calculating the probability of detecting a dark count during each 128 ps interval from the 100 Hz measured dark count rate of our detectors. It is also helpful to note that the sampling interval that we used is larger than the 68 ps jitter of our SSPD jitter, thus we have neglected the jitter in our predictions.

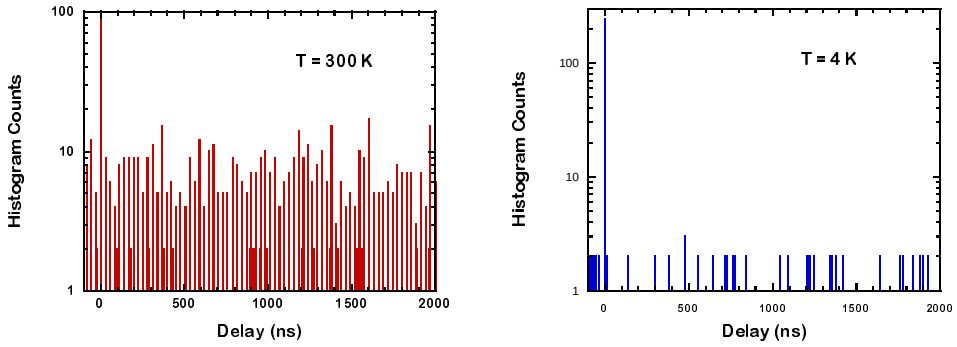

(a) (b)

Fig. 6. Histograms of the relative delay between clicks on the two detectors. At room temperature (a), we see a series of noticeable counts at a rate that is synchronous with the pump laser. When the DSF is cooled to 4 K (b), the Raman contribution is almost entirely eliminated, and the non-zero-delay counts are significantly reduced.

Table 1. Examples of possible combinations of detected clicks that yield counts at the zero-delay peak recorded by the TIA, along with the pump powers at which these counts are expected to be strong contributors.

Signal at Detector 1	Signal at Detector 2	Conditions
One half of pair #1	One half of pair #1	True coincidence; αP_0^2
One half of pair #1	Dark count	Low P_0
Dark count	One half of pair #1	Low P_0
Raman	Dark count	Low P_0
Dark count	Raman	Low P_0
One half of pair #1	Raman	Medium P_0
Raman	One half of pair #1	Medium P_0
One half of pair #1	One half of pair #2	High P_0
One half of pair #2	One half of pair #1	High P_0

We estimate the statistical uncertainty of coincidence counts as $(N_0)^{1/2}$, where N_0 is the total number of counts in the zero delay peak. Similarly, we estimate the uncertainty of the accidentals as $(\Sigma N_i - N_0)^{1/2}$, where N_i is the number of counts in each histogram peak. The estimated total uncertainty is then calculated from the estimated coincidence and accidental uncertainties through standard error-propagation techniques. The integration times are chosen such that N_0 is approximately 100 for each histogram. The histograms at the highest pump power were integrated for 500 s, and we integrate for 10 h at the lowest pump power.

A comparison of measured and predicted CARs as functions of pump power is shown in Fig. 7 for the cases where the DSF is at 4 K, 77 K, and 300 K. At high pump powers, the increased probability of multiple photon pair generation creates unwanted accidental counts. At low pump powers, the dark counts become significant compared to the coincidence counts. This leads to an optimal pump power around 6 mW (peak) for highest CAR. This optimal power does not change significantly with temperature, as shown in Fig. 7. The error bars of Fig. 7 are the statistical uncertainties, which are calculated as described above; these error bars are small enough that they are difficult to see on the log-scale plot of Fig. 7. The

#95442 - $15.00 USD Received 28 Apr 2008; revised 6 Jun 2008; accepted 16 Jun 2008; published 20 Jun 2008

maximum measured CAR is 1300 ± 70 at a fiber temperature of 4 K, 90 ± 15 at a temperature of 77 K, and 10 ± 2 at room temperature.

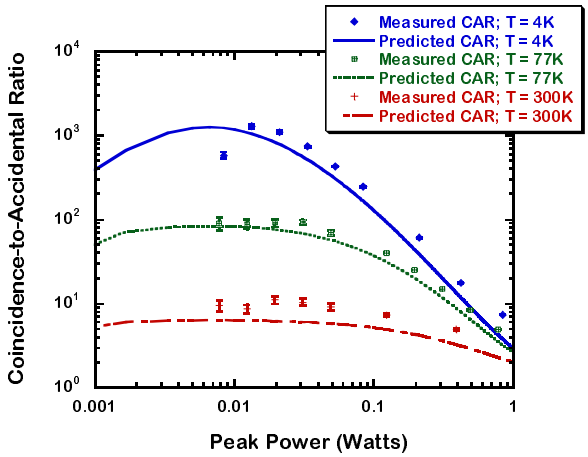

Fig. 7. Comparison of measured and predicted coincidence-to-accidental ratios. Error bars show the statistical uncertainty resulting from the practical limits to the integration time.

It is important to note that, for practical reasons, all of the curves of Figs. 6 and 7 are measured at the same pump wavelength of 1546.1 nm. From Fig. 2 we see that if we fix the pump wavelength, then the pair generation efficiency sees a noticeable change between room temperature and cryogenic temperatures. Therefore, the improved CARs measured at both 4 K and 77 K and shown in Fig. 7 compared with the room-temperature results are the result of both reduced Raman scattering and improved pair-generation efficiency. However, the effects of pump wavelength on pair-generation efficiency are weak; if we were to measure CAR with the optimal room temperature pump wavelength of 1549 nm (obtained from Fig. 2), then the room temperature CAR results would improve by only approximately 20 %. Furthermore, the fact that we fixed the pump wavelength does not impact the comparison between CARs at 4 K and 77K, because Fig. 2 shows that the optimal pump wavelength is the same for these two temperatures.

The photon-pair generation rate is 2 kHz at a pump power of 6 mW (peak) and a fiber temperature of 4 K; this is equivalent to a pair probability per pulse of $\mu = 0.00006$. However, the rate of detected photon pairs at that pump power is only 0.01 Hz, because the DEs, including filter insertion losses, are 0.001 and 0.005. Therefore, we must integrate over a period as long as 10 h in order to obtain good statistics in the histograms, particularly for the histograms at the lowest pump powers. When we pump at a peak power of 0.8 W (near the maximum for our laser and EDFA combination), we have a pair generation rate of 17 MHz and a pair probability per pulse of $\mu = 0.5$; in this case our CAR at 4 K is reduced to 7 as a result of the increased probability of multi-pair generation.

7. Summary

We have demonstrated a fiber-based photon-pair source with CAR as high as 1300, which is a factor of 12 higher than that of any of the previous reports in the telecom C-band. This can be achieved only with careful attention to all sources of background photons. We minimized the Raman contribution of the nonlinear fiber by cooling the fiber to 4 K. We also identified a Raman contribution from the short length of SMF connecting the nonlinear fiber to the rest of the system. We minimized this by configuring the system such that the last pump filter and the first of the signal and idler filters were placed as close as possible to the nonlinear fiber.

#95442 - $15.00 USD Received 28 Apr 2008; revised 6 Jun 2008; accepted 16 Jun 2008; published 20 Jun 2008

The Raman scattering in SMF and the other background photons such as ASE and 980 nm leakage are quite weak and became noticeable only after we cooled the nonlinear fiber to 4 K.

In order to optimize pair production efficiency, it is important to characterize the fiber by a stimulated FWM experiment. We described this measurement in detail, and we showed that it directly predicts the pair production efficiency. We used this classical measurement to determine the change in ZDW as a function of fiber temperature, and we demonstrated that the ZDW does not change significantly between 77 K and 4 K. The pair generation rate is relatively low (2 kHz) at the pump power that yields the highest CAR; this generation rate can be increased by increasing the pump power, but that reduces the CAR, as shown in Fig. 7.

We carefully characterized all background photon contributions and used this characterization to compare the CAR measurements with theoretical predictions, showing good agreement between the two. Our demonstration of extremely high CAR will enable low-noise photon sources to be applied to a diverse range of applications, including heralded single photons, entangled photons, and quantum-key distribution. This all-fiber photon-pair source can be readily modified to generate polarization entangled photon pairs [3-5].

Acknowledgments

We thank Jeff Van Lanen and Robert Hadfield for contributing to the design of the fiber probe used to cool the fiber to 4 K, Hiroki Takesue for valuable suggestions on the design of photon-pair sources, and John Schlager for advice regarding the properties of DSF and how to perform stimulated FWM measurements. We also thank Scott Glancy for providing helpful insight into the formulas used to predict photon-pair generation and Raman scattering, and we are grateful to Alan Migdall, Rich Mirin, and Kevin Silverman for their advice. This work was funded in part by the NIST Quantum Information Initiative.

#95442 - $15.00 USD Received 28 Apr 2008; revised 6 Jun 2008; accepted 16 Jun 2008; published 20 Jun 2008